PRACE INSTYTUTU ODLEWNICTWA
TRANSACTIONS OF FOUNDRY RESEARCH INSTITUTE

Volume LV Year 2015 Number 3

DOI: 10.7356/iod.2015.15

High-temperature oxidation of cast steel in water vapour

Wysokotemperaturowe utlenianie staliwa w parze wodnej

Renata Zapała[1], Sebastian Pach[1], Marcin Górny[1], Marta Homa[2], Aleksandra Siewiorek[2]

[1] AGH University of Science and Technology, Faculty of Foundry Engineering, Department of Cast Alloys and Composites Engineering, Reymonta 23 Str., 30-059 Krakow, Poland

[2] Foundry Research Institute, Centre for High Temperature Studies, ul. Zakopiańska 73, 30-418 Krakow, Poland

[1] AGH Akademia Górnicza-Hutnicza, Wydział Odlewnictwa, Katedra Inżynierii Stopów i Kompozytów Odlewanych, ul. Reymonta 23, 30-059 Kraków

[2] Instytut Odlewnictwa, Centrum Badań Wysokotemperaturowych, ul. Zakopiańska 73, 30-418 Kraków

E-mail: zapala@agh.edu.pl

Abstract

The article presents the results of studies of the oxidation process conducted at 900°C for 12 hours in an atmosphere of water vapour on cast heat-resistant steel with a diversified structure (ferritic-austenitic, austenitic, and austenitic with carbides). Based on the studies of oxidation kinetics, it was found that samples were oxidized in approximation with the rules of linear law. Depending on the chemical composition and structure of tested alloys, the scale formed on the alloy surface had different properties. In the tested material characterised by a ferritic-austenitic structure, the tendency of the scale to detach from the surface of the metallic substrate was observed. It was probably due to different coefficients of the thermal expansion of austenite and ferrite.

Keywords: cast heat-resistant steel, microstructure, high-temperature corrosion, water vapour

Streszczenie

Praca prezentuje wyniki badań utleniania w atmosferze pary wodnej staliwa żaroodpornego o różnej strukturze (ferrytyczno-austenitycznej, austenitycznej i austenitycznej z węglikami) w temperaturze 900°C w ciągu 12 godzin. Na podstawie badań kinetyki utleniania stwierdzono, że badane próbki utleniały się w przybliżeniu zgodnie z prawem liniowym. W zależności od składu chemicznego i struktury badanych stopów obserwowano odmienne właściwości powstałych zgorzelin. W przypadku materiału o strukturze ferrytyczno-austenitycznej stwierdzono odpadanie zgorzeliny od powierzchni rdzenia metalicznego związane prawdopodobnie z różnym współczynnikiem rozszerzalności cieplnej austenitu i ferrytu.

Słowa kluczowe: staliwo żaroodporne, mikrostruktura, korozja wysokotemperaturowa, para wodna

1. Introduction

Improving the efficiency of industrial installations in which castings are operating is associated with an increased interest in casting alloys in different grades of cast heat-resistant steel. Castings made from heat-resistant alloys can operate at high temperatures (above 600°C) and in various atmospheres (oxidising, reducing, alkaline, exhaust gases) [1−3].

The use of cast steel for high temperature applications depends on its tendency to form a compact, Cr-rich scale. Cast heat-resistant steel forms this type of scale in a moisture-free atmosphere (e.g. dry air), but when alloys containing Cr are exposed to the effect of dry gas at a temperature of about 1000°C, the resulting CrO_3 compound is deprived of its protective properties [4, 5]. On the other hand, when the atmosphere contains water vapour, this can significantly affect the process of oxidation, resulting even in a catastrophic destruction of material – all this is due to the increased rate of oxidation and rapidly growing scale, which contributes to breakaway oxidation of the alloy [5−7]. In an atmosphere containing water vapour, this phenomenon is related to the formation of rich in Fe scale showing significantly worse protective properties than the scale consisting of Cr oxides [4, 5, 8]. Furthermore, greater susceptibility of alloys to oxidation in atmospheres containing water vapour may be associated with the occurrence and evaporation of compounds such as hydroxides of Cr

and Fe, e.g. $CrO_2(OH)_2$ and $Cr(OH)_3$, and scale cracking caused by stress and resulting in an increased transport of oxygen [6, 9−12].

Protective properties of the scale are considerably reduced by high partial pressure of water vapour and a faster flow of gas [13, 14]. In [8, 15, 16], the authors have indicated that the only alternative to ensure the resistance of materials to the effect of water vapour is through the increased content of Cr (above 20−25%). Research conducted by Jurasz et al. [17] confirms this hypothesis. The X33CrNiMn23-8 steel (containing 23.5% Cr) has at 900°C better corrosion resistance in an atmosphere of steam than the X50CrMnNiNbN21-9 steel, which contains 19.9% Cr. Increasing Cr content in alloys is one of the possible strategies but it contributes significantly to the growth of costs and reduces the mechanical properties of cast steel [17]. The effect of steel oxidation in water vapour is largely dependent on such factors as Cr diffusion in the alloy, the structure of the alloy (ferritic, austenitic, ferritic-austenitic), the grain size or the degree of alloy surface deformation changing the number of grain boundaries and dislocations, acting as paths of high-speed diffusion [18, 19].

It was also found that the diversity of microstructures (the type of matrix and carbide morphology) can directly affect material properties, including resistance to the effect of atmospheric air at high temperatures. Austenitic matrix shows better heat resistance than the ferritic one, while the precipitates of Cr carbides cause impoverishment of the alloy matrix in Cr, which adversely affects the cast steel heat resistance [8].

Oxidation studies conducted for about 100 hours at a temperature of 650°C in an atmosphere containing water vapour on the alloys of Fe-12Ni-18Cr (austenitic structure) and Fe-22Cr (ferritic structure) indicate that the Fe-12Ni-18Cr alloy exhibits much greater weight gain than the Fe-22Cr alloy, but is resistant to the breakaway oxidation phenomena, and therefore it can be assumed that it will behave much better in atmospheres containing water vapour. Some attention should also be paid to the fact that increasing the Cr content in ferritic alloys improves the corrosion resistance under the above mentioned conditions [6].

Literature provides only very scarce data on the effect that the cast steel structure may have on its resistance to corrosion in an atmosphere of water vapour at high temperature. Therefore the purpose of the present study was to examine the possible impact of the cast steel structure on its resistance to corrosion in an atmosphere of water vapour at a temperature of 900°C during 12 hours. The test conditions (time and temperature) were selected based on the EN 10295:2002 standard and the maximum temperature of the tested cast steel operation in an atmosphere of air specified in this standard. Since this temperature assumes different values for different cast steel grades (900°C, 1100°C), for studies, the lowest permissible value was selected. Moreover, the range of the temperature values has been adjusted to the cast steel grade applied for parts of the specific industrial installations (e.g. petrochemical installations – cast GX40NiCrSi35-26 steel, equipment for thermal and thermo-chemical treatment – cast GX40CrNiSi27-4 and GX25CrNiSi18-9 steels). The time of the experiment adopted in this study in no way reflects the actual performance time of these materials, reaching sometimes 10 000 h. It is only meant to serve as a reference point in further studies of the behaviour of the examined cast steel grades during long-term research.

2. Test materials and methods

2.1. Test materials

For tests, three grades of cast steel differing in microstructure according to the PN-EN 10295:2004 standard were selected:

a) cast GX40CrNiSi27-4 steel – ferritic-austenitic structure,

b) cast GX25CrNiSi18-9 steel – austenitic structure,

c) cast GX40NiCrSi35-26 steel – austenitic structure with carbide precipitates.

Table 1 compares the chemical composition of the tested alloys examined with a SPECTROMAXx spectrometer (for all the investigated elements the level of significance of the measurements is ±0.001%).

Table 1. Chemical composition of the tested alloys
Tabela 1. Skład chemiczny badanych stopów

Grade/Gatunek	Chemical composition, wt.% / Skład chemiczny, % wag.							
	C	Si	Mn	P	S	Cr	Ni	Fe
GX40CrNiSi27-4	0.41	1.5	1.5	0.014	0.014	29.5	6.3	rest/reszta
GX25NiCrSi18-9	0.20	0.3	0.3	0.010	0.020	19.7	10.0	rest/reszta
GX40NiCrSi35-26	0.35	1.6	0.7	0.001	0.013	25.8	32.9	rest/reszta

2.2. Examinations of microstructure (SEM)

Microstructural examinations were made with a Neophot 32 light microscope and JOEL 5500LV scanning microscope equipped with an IXRF EDS system for the X-ray microanalysis (acceleration voltage – 20 kV). The methods of local and surface microanalysis were applied in the studies.

2.3. Studies of high-temperature corrosion

The oxidation process was carried out in an atmosphere of water vapour at a temperature of 900°C for 12 hours. The disc-shaped samples were cut out from the φ = 8 mm rods prepared earlier by turning, followed by grinding (abrasive paper of 80−1200 grit) and polishing to the, so-called, "mirror shine" (Al_2O_3). Samples were prepared in accordance with the procedure developed for materials and studies of this type [8] and were degreased before tests. Studies were conducted in an STA 449 F3 Jupiter thermoanalyser coupled with a Netzsch QMS 403 Aëolos gas analyser.

3. Results and discussion

3.1. Characteristics of the base materials

The as-cast microstructures of the tested steels are shown in Figures 1−3. The microstructure of the cast GX40CrNiSi27-4 steel includes a ferritic matrix (dark areas) and austenite grains in the form of irregular precipitates (bright areas) (Fig. 1a,b).

Based on the results of SEM examinations at points 1 and 2 (Fig. 1b), the enrichment of ferrite in Cr and its impoverishment in Ni compared to austenite were stated. Visible are also the precipitates of carbide phases at points 1 and 2 (Fig. 1c). Carbide precipitates of the first type form small "islands" inside the grains of austenite; carbides of the second type occur as eutectoid precipitates distributed along the ferrite/austenite phase boundary.

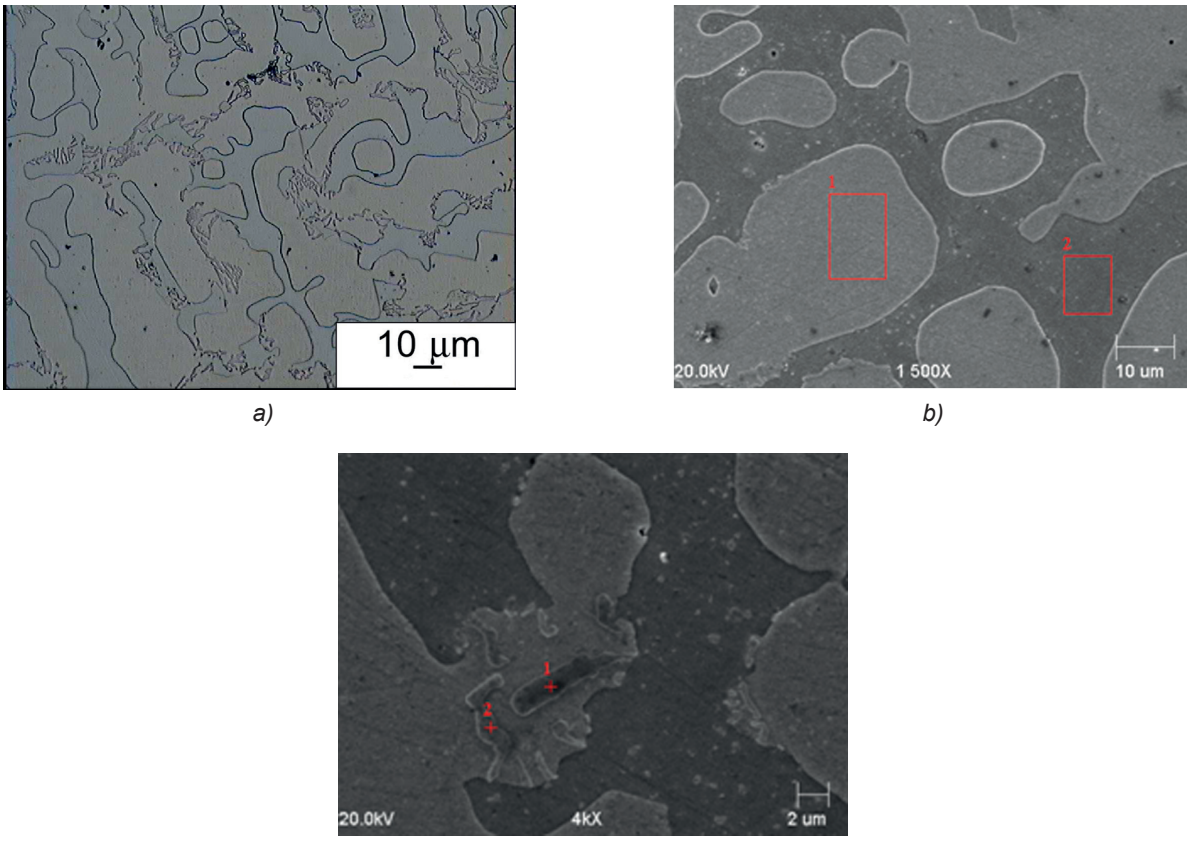

a) b)

c)

Fig. 1. As-cast microstructure of the GX40CrNiSi27-4 steel: a) optical microscope (1000×; etched with NITAL), b,c) SEM-EDS microscope with chemical analysis in regions 1 and 2

Rys. 1. Mikrostruktura staliwa GX40CrNiSi27-4 w stanie lanym: a) mikroskop optyczny (powiększenie 1000×, odczynnik: NITAL), b,c) mikroskop SEM-EDS wraz z analizą składu chemicznego w obszarach 1 i 2

The data published in the reference literature clearly state that in the tested alloys there are two types of Cr carbides, i.e. $M_{23}C_6$ and M_7C_3 [1,2,20,21]. The precipitates of carbides present in the examined cast steel contain, besides Cr (51−57 wt.%), also Fe (14−21 wt.%) (Table 2). Large differences in the content of elements in the areas where measurements have been taken may result from the fact that in the adopted measurement procedure carbon is described only as an estimated value.

Figure 2 shows the microstructure of the cast GX-25CrNiSi18-9 steel. From the image it follows that the tested material has an austenitic structure. On the austenite grain boundaries there are scarce small precipitates containing Cr in their composition. These are probably the precipitates of Cr carbides. The microstructure also contains numerous precipitates of oxides and oxide-sulphides.

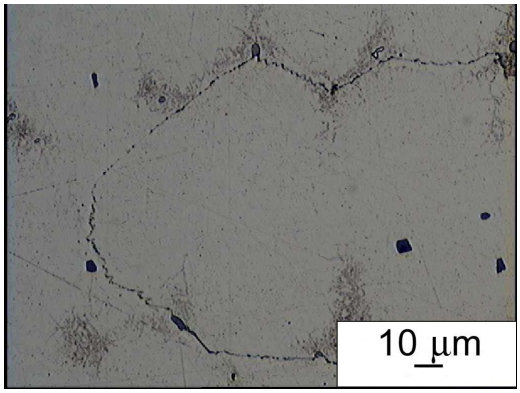

Fig. 2. As-cast microstructure of the GX25CrNiSi18-9 steel, optical microscope (1000×, etched with NITAL)

Rys. 2. Mikrostruktura staliwa GX25CrNiSi18-9 w stanie lanym, mikroskop optyczny (powiększenie 1000× odczynnik: NITAL)

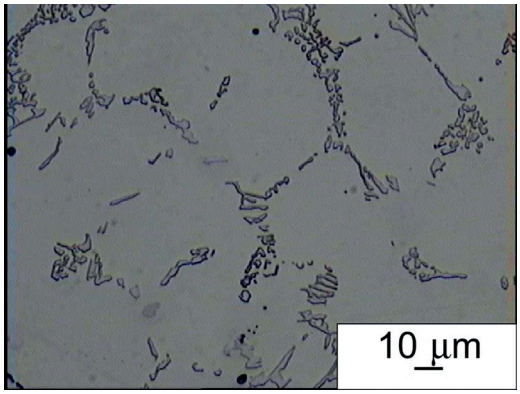

a)

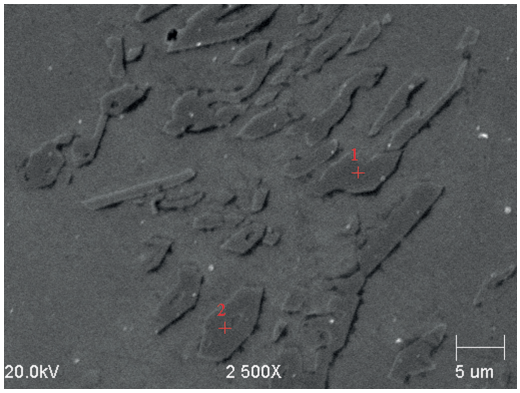

b)

Fig. 3. As-cast microstructure of the GX40CrNiSi35-26 steel: a) optical microscope (1000× etched with NITAL), b) SEM-EDS microscope with chemical analysis in regions 1 and 2

Rys. 3. Mikrostruktura staliwa GX40CrNiSi35-26 w stanie lanym: a) mikroskop optyczny (powiększenie 1000× odczynnik: NITAL), b) mikroskop SEM-EDS wraz z analizą składu chemicznego w obszarach 1 i 2

Table 2. Chemical composition in regions 1 and 2 shown in Figure 1b and 1c

Tabela 2. Analiza składu chemicznego obszarów 1 i 2 przedstawionych na rysunku 1b i 1c

Region/Obszar	Chemical composition, wt.% / Skład chemiczny, % wag.					
	Si	Cr	Mn	Fe	Ni	C
Fig. 1b)_1	2.0 ±0.4	24.20 ±1.6	–	67.20 ±3.3	6.6 ±1.2	–
Fig. 1b)_2	2.6 ±0.5	28.50 ±1.6	0.9 ±0.3	63.50 ±3.1	4.5 ±1.0	–
Fig. 1c)_1	–	57.67 ±2.3	–	13.95 ±1.4	–	28.38 ±4.3
Fig. 1c)_2	–	51.21 ±2.2	–	21.20 ±1.7	–	27.59 ±4.4

Table 3. Chemical composition in regions 1 and 2 shown in Figure 3b

Tabela 3. Analiza składu chemicznego obszarów 1 i 2 przedstawionych na rysunku 3b

Region/Obszar	Chemical composition, wt.% / Skład chemiczny, % wag.		
	Cr	Fe	C
1	70.65 ±2.7	15.15 ±1.5	14.20 ±3.4
2	71.86 ±2.7	11.00 ±1.3	17.19 ±3.6

The GX40CrNiSi35-26 alloy is characterised by an austenitic matrix (Fig. 3). In the intergranular areas, the presence of numerous, large, lamellar eutectic-like precipitates was noticed (Fig. 3a). Chemical analysis revealed in the precipitates the presence of the following elements: Cr (70−72 wt.%), Fe (11−15 wt.%) and large amounts of C (14−17 wt.%) (Table 3). From the data available in the literature it can be concluded that these are the primary precipitates of complex Cr carbides, probably of the M_7C_3 type, which are usually formed in as-cast state in alloys deprived of the elements showing higher affinity for C than Cr, e.g. Nb, Ti [22−25].

Studies of the oxidation kinetics

Figure 4 presents a collective graph showing oxidation kinetics of the examined cast steel grades in an atmosphere of water vapour at a temperature of 900°C during 12 hours.

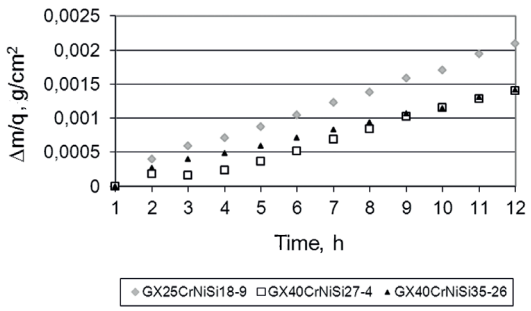

Fig. 4. Plotted kinetics of the cast steel oxidation in an atmosphere of water vapour at a temperature of 900°C

Rys. 4. Przebieg kinetyk utleniania staliwa w atmosferze pary wodnej w temperaturze 900°C

Studies have shown that the oxidation curves follow in approximation with the rules of linear law.

The curve of the oxidation kinetics of the cast GX-40CrNiSi27-4 steel shows two different periods: the first period lasting about 3 hours starts at the beginning of the measurement and is independent of the time of heating the furnace to the test temperature (about 1 hour); the second period takes time until the end of the measurement.

The process of the cast GX40CrNiSi35-26 steel oxidation is characterised by some irregularities which occur at the initial stage (until hour 4 of the experiment) and after roughly 11 hours of oxidation (a sharp increase in weight). To eliminate (or confirm) the unusual behaviour of this material, two measurements were taken – the irregularities appeared on both plotted curves.

The irregularities visible on the curves of the oxidation kinetics may be due to casting defects which occur in the tested material and require additional measurements taken on samples of the same chemical composition but at different places in the casting.

The largest increase in weight was noticed in the cast GX25CrNiSi18-9 steel (0.0021 g/cm^2) and the smallest in the cast GX40CrNiSi35-26 steel (0.0011 g/cm^2). It can be assumed that it is due to the heterogeneity of cast materials.

Table 4 compares the constant rates of corrosion reaction in the examined cast steel in an atmosphere of water vapour at a temperature of 900°C. Additionally, the table contains calculated values of the power exponents. For the tested materials, the exponent *n* assumes the values from 0.48 to 1.00.

3.2. Characteristics of the obtained scale

The images of samples after the kinetic studies are presented in Figure 5, while Figures 6−8 show the results of examinations of the sample scale morphology completed by light microscopy and SEM.

Studies show that scale formed on the cast GX-40CrNiSi27-4 steel tends to detach from the metallic substrate. After detachment of the scale, the surface is characterised by different colours from light grey to red.

Table 4. Constant corrosion rates in an atmosphere of water vapour and calculated values of the exponent n compared for the tested cast steel at 900°C

Tabela 4. Zestawienie wartości stałej szybkości korozji w atmosferze pary wodnej i współczynnika n dla badanego staliwa w temperaturze 900°C

Grade/Gatunek	**Values of constant corrosion rate, k_l, g/cm^2 · s / Wartości stałej szybkości korozji, k_l, g/cm^2 · s**	**Exponent, *n** / Współczynnik *n****
GX40CrNiSi27-4	$3.25 \cdot 10^{-8}$	0.64
GX25CrNiSi18-9	$4.84 \cdot 10^{-8}$	1.00
GX40NiCrSi35-26	$2.62 \cdot 10^{-8}$	0.48
* determined for the angle of inclination of the curves of oxidation kinetics plotted in a log-log system according to [8] / wyznaczony z kąta nachylenia wykresów kinetyki utleniania przedstawionych w układzie podwójnie logarytmicznym wg [8]		

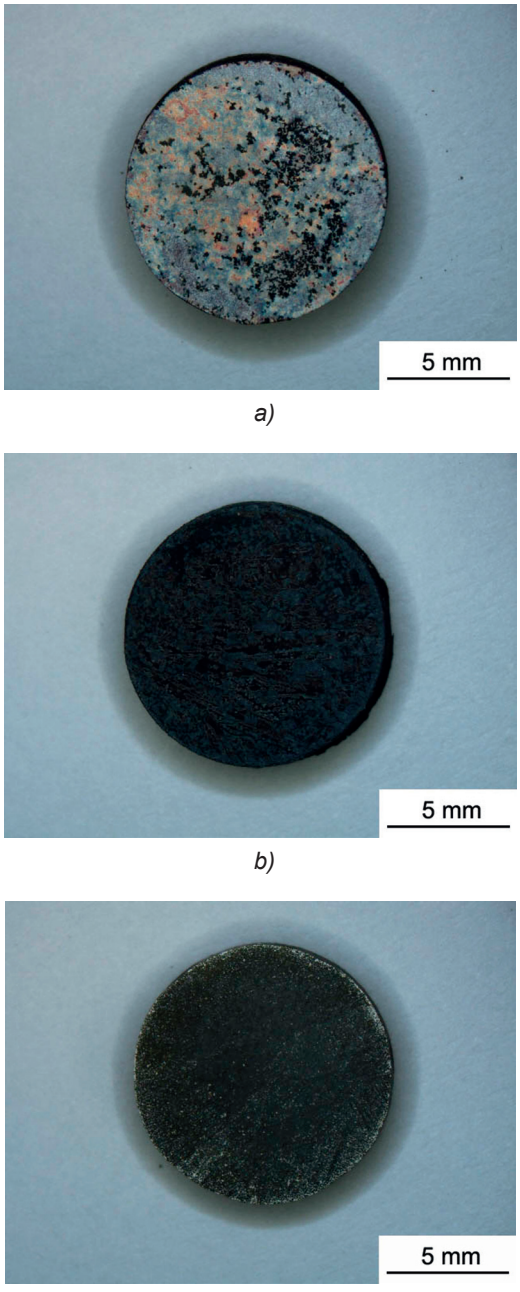

Fig. 5. The surface of cast steel samples after high-temperature studies of the oxidation process in an atmosphere of water vapour at a temperature of 900˚C during the time of 12 hours (10×), optical microscope: a) GX40CrNiSi27-4, b) GX25CrNiSi18-9, c) GX40NiCrSi35-26

Rys. 5. Powierzchnia próbek staliw po badaniach wysokotemperaturowego utleniania w atmosferze pary wodnej w temperaturze 900°C w czasie 12 godzin (pow. 10×), mikroskop optyczny: a) GX40CrNiSi27-4, b) GX25CrNiSi18-9, c) GX40CrNiSi35-26

This effect is usually associated with the presence of Fe oxides formed in the scale (e.g. Fe_2O_3 – red haematite). Another reason for the scale detachment may be the difference in the coefficients of thermal expansion of the metal and scale. The tested material is characterised by an austenitic-ferritic structure. The coefficients of the thermal expansion of ferrite ($11 \cdot 10^{-6}°C^{-1}$) and austenite ($17 \cdot 10^{-6}°C^{-1}$) are different, as are the coefficients of the thermal expansion of the products of reaction (Cr oxides ~5−7 · $10^{-6}°C^{-1}$, Fe oxides ~8−15 · $10^{-6}°C^{-1}$ and spinels ~7 · $10^{-6}°C^{-1}$) [26−30]. As a consequence, during cooling of the alloy, some stresses may arise and destroy the bond between the scale and the substrate.

In samples of the cast GX40CrNiSi27-4 steel, two characteristic areas have been distinguished, i.e. the area with the remaining fragments of the corrugated scale which tends to fall off (areas 1 and 2 in Figure 6, Table 5) – containing Cr, Mn and O_2 as well as small amounts of Fe, and probably of Cr_2O_3 and $MnCr_2O_4$, and the area free from the scale (area 3 in Figure 6, Table 5) – containing mainly Fe (~ 70%) with a low content of oxygen (compared to the area with the scale).

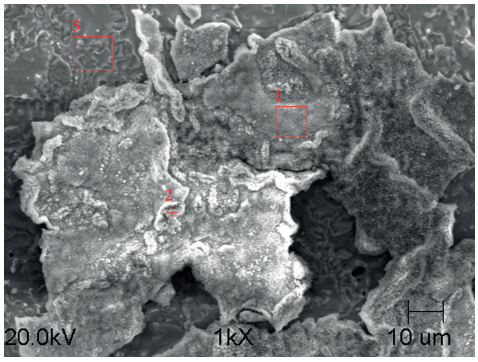

Fig. 6. Microstructure of scale formed on the cast GX40CrNiSi27-4 steel with chemical analysis in regions 1, 2 and 3

Rys. 6. Mikrostruktura zgorzeliny staliwa GX40CrNiSi27-4 wraz z analizą składu chemicznego w obszarach 1, 2 i 3

Compared to the cast GX40CrNiSi27-4 steel, the scale formed on the cast GX25CrNiSi18-9 steel shows much better adhesion to the substrate and is more compact (Fig. 5b). Better adhesion of the scale is probably due to a monophase structure of the material (it eliminates stresses resulting from the diversified phase composition). SEM observations of the scale formed on the surface of the samples of the cast GX25CrNiSi18-9 steel (Fig. 7a−c) have revealed three different areas: the bright area (Fig. 7a, Table 6) enriched in Fe and O_2, the dark area (Fig. 7b, Table 6) enriched in Cr, Fe and O_2, doped with Ni and Mn, and the intermediate area (Fig. 7c, Table 6) enriched in Fe, Cr and O_2 (but of a composition different than the area mentioned previously) doped with Ni (Table 6).

Chemical analysis of the examined scale confirmed the data available in the literature [14,31]. Based on these results it can be concluded that the scale formed in alloys containing 14−20% Cr is of a complex nature. The outer layer is composed of haematite, while the inner layer is a complex spinel containing Fe, Cr, Ni, and O.

Table 5. Chemical analysis in regions 1, 2 and 3 shown in Figure 6

Tabela 5. Analiza składu chemicznego obszarów 1, 2 i 3 przedstawionych na rysunku 6

Region/ Obszar	Chemical composition, wt% / Skład chemiczny, % wag.					
	O	Si	Cr	Mn	Fe	Ni
Fig. 6_1	35.7 ±1.0	–	52.3 ±1.3	10.2 ±0.7	1.4 ±0.4	0.3 ±0.1
Fig. 6_2	37.9 ±1.0	0.2 ±0.1	39.1 ±1.1	20.9 ±0.9	1.7 ±0.3	0.2 ±0.1
Fig. 6_3	4.9 ±0.4	1.5 ±0.2	14.7 ±0.6	0.2 ±0.1	70.4 ±1.8	8.4 ±0.7

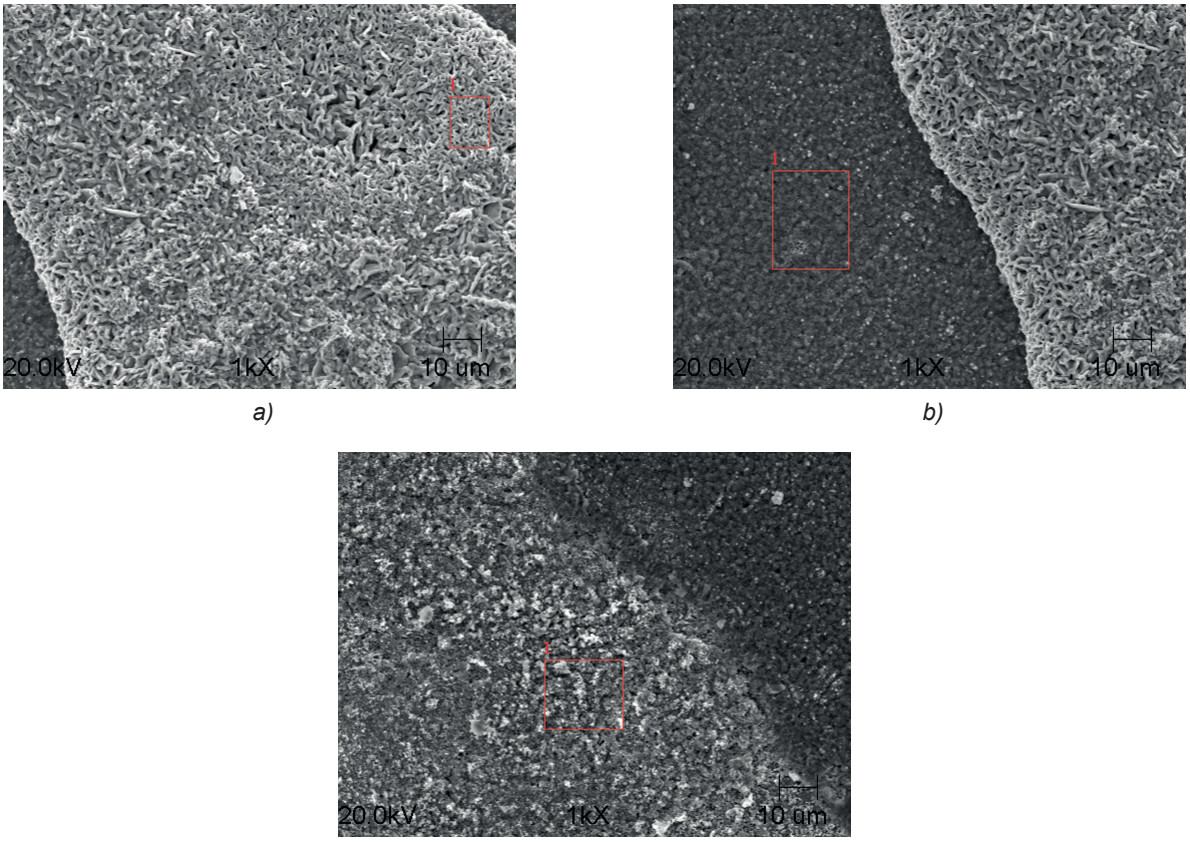

a) *b)* *c)*

Fig. 7. Microstructure of scale formed on the cast GX25CrNiSi18-9 steel: a) bright area, b) dark area with the chemical analysis in marked regions, c) intermediate area

Rys. 7. Mikrostruktura zgorzeliny staliwa GX25CrNiSi18-9: a) obszar jasny, b) obszar ciemny wraz z analizą składu chemicznego w zaznaczonych obszarach, c) obszar pośredni

Table 6. Chemical analysis in regions 1, 2 and 3 shown in Figure 7a, b, c

Tabela 6. Analiza składu chemicznego obszarów 1, 2 i 3 przedstawionych na rysunku 7a, b, c

Region/Obszar	Chemical composition, wt.% / Skład chemiczny, % wag.					
	O	Si	Cr	Mn	Fe	Ni
Fig. 7a)_1	27.8 ±1.0	0.3 ±0.1	0.7 ±0.1	0.3 ±0.1	70.5 ±1.8	0.4 ±0.2
Fig. 7b)_1	31.0 ±1.0	1.0 ±0.1	38.2 ±1.1	0.4 ±0.1	26.4 ±1.1	3.0 ±0.4
Fig. 7c)_1	27.5 ±1.0	0.5 ±0.1	28.4 ±1.0	–	39.0 ±1.4	4.4 ±0.6

Table 7. Chemical analysis in the regions shown in Figures 8a and 8b
Tabela 7. Analiza składu chemicznego obszarów przedstawionych na rysunku 8a i 8b

Region/Obszar	Chemical composition, wt.% / Skład chemiczny, % wag.					
	O	Si	Cr	Mn	Fe	Ni
Fig. 8a)_1	33.6 ±1.0	1.7 ±0.3	44.4 ±1.2	7.0 ±0.5	8.0 ±0.7	5.2 ±0.7
Fig. 8a)_2	34.3 ±1.0	0.3 ±0.2	56.2 ±1.4	3.7 ±0.4	3.1 ±0.5	2.5 ±0.5
Fig. 8a)_3	31.2 ±1.0	–	12.0 ±0.6	54.0 ±1.5	1.9 ±0.4	0.8 ±0.4
Fig. 8b)_1	29.9 ±1.1	0.7 ±0.2	4.6 ±0.4	63.5 ±1.7	1.3 ±0.4	–

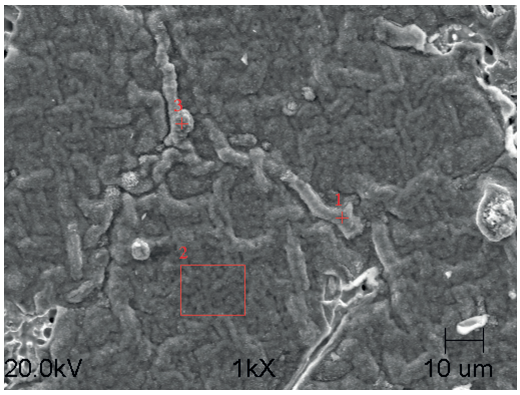

a)

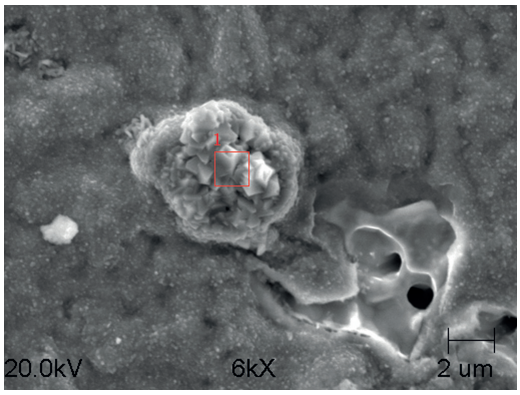

b)

Fig. 8a,b. Microstructure of scale formed on the cast GX40NiCrSi35-26 steel with the results of chemical analysis, SEM-EDS
Rys. 8a,b. Mikrostruktura zgorzeliny staliwa GX40NiCrSi35-26 wraz z wynikami analizy składu chemicznego, SEM-EDS

Of all the tested samples, the scale formed on the cast GX40NiCrSi35-26 steel is characterised by the best adhesion to the substrate and completely covers the metallic core (Fig. 5c), forming a well adhering protective film. This is related with the alloy composition (the highest, among all the tested materials, content of alloying elements such as Cr), and a homogeneous austenitic matrix. SEM examinations showed the surface of the cast GX40NiCrSi35-26 steel covered with well adhering scale composed of fine crystalline products (Fig. 8a). Some pores, however, were noted at the boundaries where carbide precipitates have occured as shown in Figure 8b.

EDS analysis in selected areas shows that, depending on the chemical composition, the scale formed on the cast steel surface can be divided into the scale rich in Cr and O_2 – probably forming Cr_2O_3 (areas 1 and 2 in Fig. 8a, Table 7) and the scale rich in Cr, Mn and O_2 (point 3 in Fig. 8a and point 1 in Fig. 8b, Table 7) – the elements that are also found in the composition of the $MnCr_2O_4$ spinel forming fine spherical "blooms".

The available literature data [15−18] indicate that it is the spinel formed on Cr steels that protects the steel surface from the formation of a volatile CrO_3 compound.

4. Conclusions

The obtained results enable drawing the following conclusions:

1. The kinetics of the reaction taking place in the examined alloys in an atmosphere of water vapour at a temperature of 900°C during 12 hours assumes the course which, in approximation, can be described by linear law. The kinetics closest to the perfect run has been observed in the cast GX25CrNiSi18-9 steel.

2. The rate of the high-temperature corrosion process taking place in samples of the cast GX40CrNiSi27-4, GX25CrNiSi18-9 and GX40CrNiSi35-26 steels oxidised in an atmosphere of water vapour at a temperature of 900°C during 12 hours is independent of the alloy structure – no significant differences have been observed in the values of k_l.

3. The scale formed on the cast GX40CrNiSi27-4 steel tends to detach from the substrate, which is probably due to the effect of stresses arising during cooling of the two-phase material.

4. Chemical analysis of scale formed on the cast GX40CrNiSi27-4 steel has revealed the presence of Cr, Mn, O, and small amounts of Fe. Areas not coated by the scale (prevailing on the sample) were rich in Fe (about 70%) and O.

5. The scale formed on the cast GX25CrNiSi18-9 steel is characterised by much better adhesion to the base material than the scale formed on the cast GX40CrNiSi27-4 steel. The examined scale has a complex structure – the outer layer is composed of Fe and O, while the inner layer is composed of spinel containing Fe, Cr, Ni and O.

6. Of all the tested samples of the scale, the scale formed on the cast GX40CrNiSi35-26 steel is characterised by the best adhesion to the base material, and completely covers the metallic core.

7. Chemical analysis of scale formed on the cast GX40CrNiSi35-26 steel has proved its enrichment in Cr and O, showing also the presence of small spherical products – probably the $MnCr_2O_4$ spinel.

Acknowledgements

Thermogravimetric studies were carried out within the project No. 2015/00 entitled “Application of coupled thermogravimetric analysis (TG / DTA / DSC) and SPM analysis to study the mechanism of high-temperature corrosion in selected grades of steel” on the device purchased as part of a structural project No. POIG.02.02.00-00-012/08 entitled: “Retrofitting the research infrastructure of the Malopolska Centre for Innovative Technologies and Materials”.

References

1. Głownia, J. (2002). *Odlewy ze stali stopowej – zastosowanie*. Kraków: Fotobit.
2. PN-EN 10295:2004 – Odlewy ze staliwa żaroodpornego.
3. Dobrzański, L. (red.). (2011). *Leksykon materiałoznawstwa. Tom 1*. Warszawa: Verlag Dashofer.
4. Kofstad, P. (1988). *High temperature corrosion*. London: Elsevier Applied Science.
5. Sultan, A., Karakaya, I., Erdoğan, M. (2012). Influence of water vapour on high temperature oxidation of steels used in petroleum refinery heaters. *Mater. Corros.*, *63*(2), 119−126.
6. Mu, N., Jung, K.Y., Yanar, N.M., Meier, G.H., Pettit, F.S., Holcomb, G.R. (2012). Water vapor effects on the oxidation behavior of Fe–Cr and Ni–Cr alloys in atmospheres relevant to oxy-fuel combustion. *Oxid. Met.*, *78*(3), 221−237.
7. Douglass, D.L., Kofstad, P., Rahmel, A., Wood, G.C. (1996). International workshop on high-temperature corrosion. *Oxid. Met.*, *45*(5−6), 529−620.
8. Mrowiec, S. (1982). *Kinetyka i mechanizm utleniania metali*. Katowice: Śląsk.
9. Asteman, H., Svensson, J.E., Johansson L.G. (2002). Evidence for chromium evaporation influencing the oxidation of 304L. The effect of temperature and flow rate. *Oxid. Met.*, *57*(3−4), 193−216.
10. Asteman, H., Svensson, J.E., Johansson, L.G., Norell, M. (1999). Indication of chromium oxide hydroxide evaporation during oxidation of 304L at 873 K in the presence of 10% water vapour. *Oxid. Met.*, *52*(1−2), 95−111.
11. Asteman, H., Svensson, J.E., Norell, M., Johansson, L.G. (2000). Influence of water vapour and flow rate on the high-temperature oxidation of 304L. Effect of chromium oxide hydroxide evaporation. *Oxid. Met.*, *54*(1−2), 11−26.
12. Ehlers, J., Young, D.J., Smaardijk, E.J., Tyagi, A.K., Penkalla, H.J., Singheiser, L., Quadakkers, W.J. (2006). Enhanced oxidation of the 9% Cr steel P91 in water vapour containing environments. *Corros. Sci.*, *48*(11), 3428−3454.
13. Rakowski, J.M., Pint, B. (2000). Observations on the effect of water vapour on the elevated temperature oxidation of austenitic stainless steel foil. *Proceedings of Corrosion 2000*, NACE Paper 00-517.
14. Mrowec, S., Werber, T. (1974). *Korozja gazowa metali*. Katowice: Śląsk.
15. Pint, B., Rakowski, J.M. (2000). *Effect of water vapour on the oxidation resistance of stainless steels*. Presented at NACE Corrosion 2000, Orlando, NACE Paper 00-259, 1−14.
16. Otsuka, N., Shida, Y., Fujikawa, H. (1989). Internal-external transition for the oxidation of Fe-Cr-Ni austenitic stainless steels in steam. *Oxid. Metals*, *32*(1−2), 13−45.
17. Jurasz, Z., Adamaszek, K., Janik, R., Grzesik, Z., Mrowec, S. (2009). High temperature corrosion of valve steels in atmosphere containing water vapour. *J. Solid State Electrochem.*, *13*(11), 1709−1714.
18. Piehl, C., Tökei, Z., Grabke, H.J. (2001). Surface treatment and cold working as tools to improve oxidation behaviour of chromium steels. *Mater. Sci. Forum*, *369−372*, 319−326.
19. Peraldi, R., Pint, B.A. (2004). Effect of Cr and Ni contents on the oxidation behaviour of ferritic and austenitic model alloys in air with water vapour. *Oxid. Met.*, *61*(5−6), 463−483.
20. Restrepo Garcés, G., Le Cose, J., Garin, J.L., Mannheim, R.L. (2004). σ-phase precipitation in two heat-resistant steels – influence of carbides and microstructure. *Scripta Mater.*, *50*(5), 651−654.
21. Garin, J.L., Mannheim, R.L. (2009). Sigma-phase precipitation upon industrial-like heating of cast heat-resistant steels. *J. Mater. Proces. Tech.*, *209*(7), 3143−3148.
22. Przybyłowicz, K. (2003). *Metaloznawstwo*. Warszawa: Wydawnictwa Naukowo-Techniczne.

23. Sourmail, T. (2001). Precipitation in creep resistant austenitic stainless steels. *Mater. Sci. Tech.*, *17,* 1−14.
24. Barbabela, G.D., de Almeida, L.H., da Silveira, T.L., Le May, I. (1991). Phase characterization in two centrifugally cast HK stainless steel tubes. *Mater. Charact.*, *26*(1), 1−7.
25. de Almeida Soares, G.D., de Almeida, L.H., de Silveira, T.L., Le May, I. (1992). Niobium additions in HP heat resistant cast steels. *Mater. Charact.*, *29*(3), 387−396.
26. Callister, W.D. (2003). *Materials science and engineering. An introduction*. 6th edition. Hoboken: John Wiley& Sons, Inc.
27. Taneichi, K., Narushima, T., Iguchi, Y., Ouchi, C. (2006). Oxidation or nitridation behavior of pure chromium and chromium alloys containing 10 mass%Ni or Fe in atmospheric heating. *Mater. Trans., 47*(10), 2540−2546.
28. Pang, X., Gao, K., Yang, H., Qiao, L., Wang, Y., Volinsky, A.A. (2007). Interfacial microstructure of chromium oxide coatings. *Adv. Eng. Mater.*, *9*(7), 594−599.
29. Takeda, M., Onishi, T., Nakakubo, S., Fujimoto, S. (2009). Physical properties of iron-oxide scales on Si-containing steels at high temperature. *Mater. Trans.*, *50*(9), 2242−2246.
30. Qu, W., Jian, L., Hill, J.M., Ivey, D.G. (2006). Electrical and microstructural characterization of spinel phases as potential coatings for SOFC metallic interconnects. *J. Power Sources*, *53*(1), 114−124.
31. Mrowiec, S., Werber, T. (1968). *Nowoczesne materiały żaroodporne*. Warszawa: Wydawnictwa Naukowo-Techniczne.